Journal of Structural Biology 181 (2013) 95–107

Contents lists available at SciVerse ScienceDirect

Journal of Structural Biology

journal homepage: www.elsevier.com/locate/yjsbi

Secondary osteon size and collagen/lamellar organization (“osteon morphotypes”) are not coupled, but potentially adapt independently for local strain mode or magnitude

John G. Skedros *, Kendra E. Keenan, Tyler J. Williams, Casey J. Kiser

Bone and Joint Research Laboratory, Department of Veterans Affairs Medical Center, Salt Lake City, UT, USA
The University of Utah Department of Orthopedic Surgery, Salt Lake City, UT, USA

ARTICLE INFO

Article history:
Received 25 June 2012
Received in revised form 27 September 2012
Accepted 8 October 2012
Available online 1 November 2012

Keywords:
Osteon
Collagen orientation
Strain mode
Strain magnitude
Bone adaptation
Chimpanzee femur
Human femur
Deer calcaneus
Equine calcaneus
Equine radius
Sheep radius

ABSTRACT

In bone, matrix slippage that occurs at cement lines of secondary osteons during loading is an important toughening mechanism. Toughness can also be enhanced by modifications in osteon cross-sectional size (diameter) for specific load environments; for example, smaller osteons in more highly strained “compression” regions *vs.* larger osteons in less strained “tension” regions. Additional osteon characteristics that enhance toughness are distinctive variations in collagen/lamellar organization (i.e., “osteon morphotypes”). Interactions might exist between osteon diameter and morphotype that represent adaptations for resisting deleterious shear stresses that occur at the cement line. This may be why osteons often have a peripheral ring (or “hoop”) of highly oblique/transverse collagen. We hypothesized that well developed/distinct “hoops” are compensatory adaptations in cases where increased osteon diameter is mechanically advantageous (e.g., larger osteons in “tension” regions would have well developed/distinct “hoops” in order to resist deleterious consequences of co-existing localized shear stresses). We tested this hypothesis by determining if there are correlations between osteon diameters and strongly hooped morphotypes in “tension”, “compression”, and “neutral axis” regions of femora (chimpanzees, humans), radii (horse, sheep) and calcanei (horse, deer). The results reject the hypothesis—larger osteons are not associated with well developed/distinct “hoops”, even in “tension regions” where the effect was expected to be obvious. Although osteon diameter and morphotype are not coupled, osteon diameters seem to be associated with increased strain magnitudes in some cases, but this is inconsistent. By contrast, osteon morphotypes are more strongly correlated with the distribution of tension and compression.

Published by Elsevier Inc.

1. Introduction

One beneficial result of remodeling of compact (cortical) bone with secondary osteons (Haversian systems) in non-elderly individuals is that tissue mechanical properties, especially fatigue resistance and toughness,[1] can be improved by the introduction of osteonal interfaces, including cement lines and interlamellar seams (Launey et al., 2010a; Nalla et al., 2005a,b; Skedros et al., 2005). In this context, the mechanical benefits of increased concentrations of secondary osteons have been compared to the fibers in a fiber-reinforced ceramic matrix composite material (Doblaré et al., 2004; Hogan, 1992; Martin et al., 1998; Mohsin et al., 2006; Najafi et al., 2009; Yeni et al., 1997). An important observation is the finding that the population densities of osteons with specific patterns of lamellar and collagen organization are increased in loading environments that are characterized by local prevalence/predominance of a specific strain mode (tension, compression, or shear) (Riggs et al., 1993a; Skedros, 2012; Skedros et al., 2009, 2011a). Hence, in addition to the potential for modifying the presence and complexity of their interfaces (Crescimanno and Stout, 2012; Keenan et al., 2010; Robling and Stout, 1999; Skedros et al., 2007a), matrix organization of osteons can be modified in ways that are mechanically adaptive. These specific osteon “types” have been described as “osteon morphotypes”; this characterization is largely based on the

* Corresponding author. Address: 5323 South Woodrow Street, Suite 200, Salt Lake City, UT 84107, USA. Fax: +1 801 747 1023.
E-mail address: jskedrosmd@uosmd.com (J.G. Skedros).

[1] Toughness refers to the amount of energy required to fracture a material; the more the overall amount of energy consumed, the ‘tougher’ the material (Zioupos and Currey, 1998). Tough materials resist damage propagation but do not necessarily resist damage formation. Toughness tests typically involve propagating a crack in a controlled direction through a specimen machined into a specific shape for this test. Toughness measurements obtained from these ‘formal’ toughness tests are different from the ‘toughness’ that is often ‘informally’ used (as in this study) to describe the energy absorbed by a specimen during a more conventional failure test. In this case, energy absorption is measured as the area under the stress/strain curve (Turner and Burr, 1993), which is an indirect measure of propagation toughness (Vashishth, 2004).

1047-8477/$ - see front matter Published by Elsevier Inc.
http://dx.doi.org/10.1016/j.jsb.2012.10.013

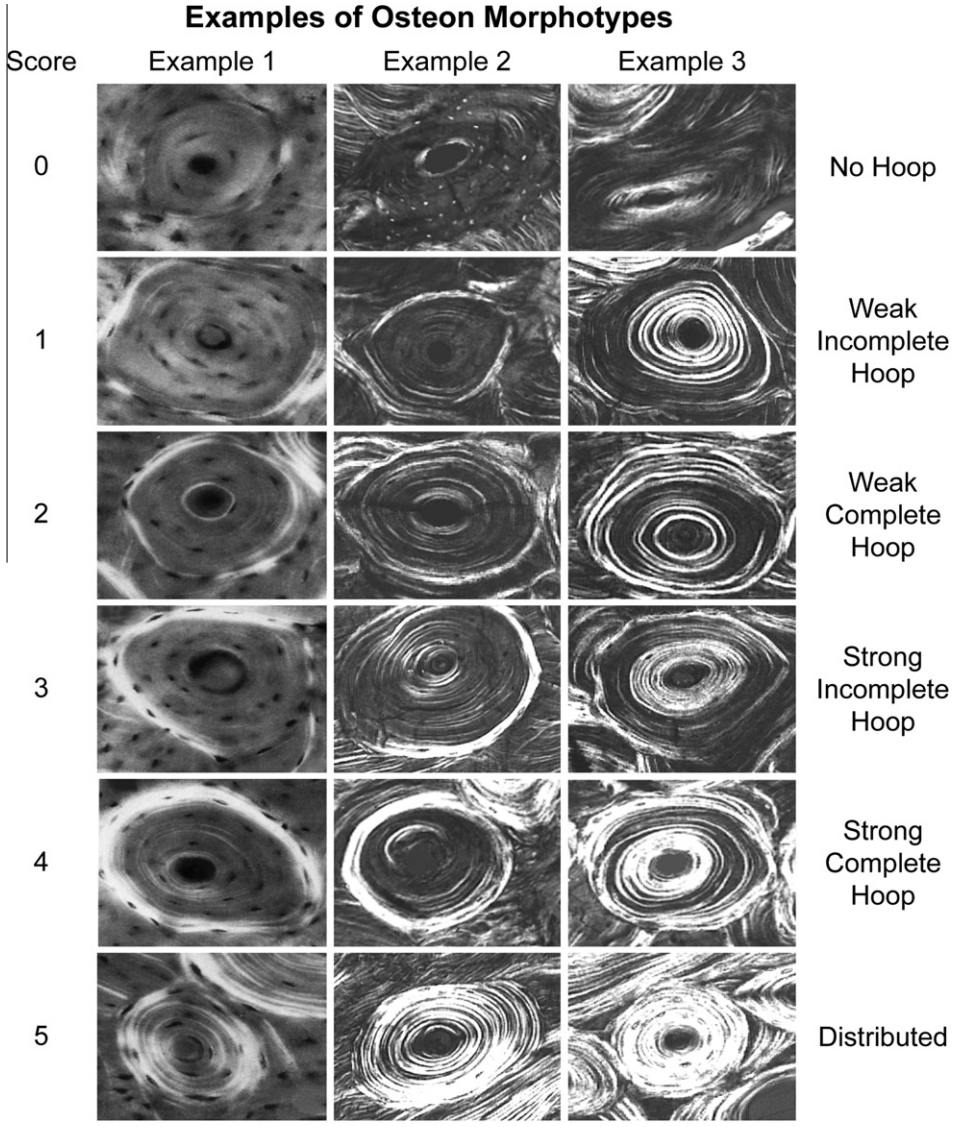

Fig.1. The six-point morphotype scoring schemes with three examples of each birefringence pattern (“morphotype”) in circular polarized light. The images in the left column are reproduced from the original study of Martin et al. (1996) but are re-ordered to conform with the 6-point scoring scheme reported in Skedros et al. (2009). The osteons from the middle and right columns are from chimpanzee femora (Skedros et al., 2011b). Also shown in columns 2 and 3 are some osteon “hybrids” (i.e., with characteristics of distributed/alternating and hooped morphotypes) (described in Skedros et al. (2011b)), some of which might be well suited for accommodating heterogeneous strains produced by variable/complex loading environments. The six-point scoring scheme that is described in these previous studies is based on the birefringence (weak *vs.* strong) and completeness of the peripheral lamella or “hoop”. In this scheme the acronyms mean that the peripheral “hoop” is: O = complete and strong, OI = incomplete and strong, OW = is complete and weak, and OWI = incomplete and weak. The morphotype “scores” are then: 0 = category N, a dark osteon with no birefringent (bright) hoop; 1 = category OWI, a combination of OI and OW; 2 = category OW, similar to O but the birefringent peripheral hoop is weak; 3 = category OI, similar to O but the birefringent peripheral hoop is incomplete; 4 = category O osteon with a strongly birefringent peripheral hoop; 5 = category D, birefringent lamellae are distributed throughout the wall of the osteon (“distributed” osteon group). This group includes “bright” osteons (less frequent) and “alternating” osteons (more frequent).

completeness and intensity of birefringent rings (or “hoops”) that often occur at their periphery, as seen in circularly polarized light (CPL) images of thin transverse sections (Fig. 1) (Skedros et al., 2011b). The increased birefringence appears as brighter (whiter) gray levels in grayscale CPL images, and this correlates with increased oblique-to-transverse collagen fiber orientation (CFO) (in CPL longitudinal CFO appears dark; compare scores 0 and 5 in Fig. 1) (Boyde and Riggs, 1990; Bromage et al., 2003; Skedros et al., 2009).

When compared to osteons in “compression regions” of bones habitually loaded in bending, “tension regions” have osteon morphotypes with more longitudinal collagen in the majority of their wall and with some degree of peripheral “hoopedness” (i.e., completeness and brightness intensity of a peripheral “hoop” in CPL images; scores 1–4 in Fig. 1). A composite osteon morphotype score (MTS) has been described that strongly correlates with the average CFO of an entire microscopic image (Skedros et al., 2011a,b), which in turn correlates with the toughness of the bone (Riggs et al., 1993b; Skedros et al., 2006). Consequently, osteon MTSs can be used as an index for identifying microstructural adaptations and may act to enhance toughness for regional variations in habitual strain mode.

In cortical bone, regional strain-mode-specific toughness can also be enhanced by modifications in osteon cross-sectional size. This is indirectly supported by data showing that in some bones smaller osteons occur in regions that receive a history of prevalent/predominant compression (usually higher strains) compared to regions that receive prevalent/predominant tension (usually

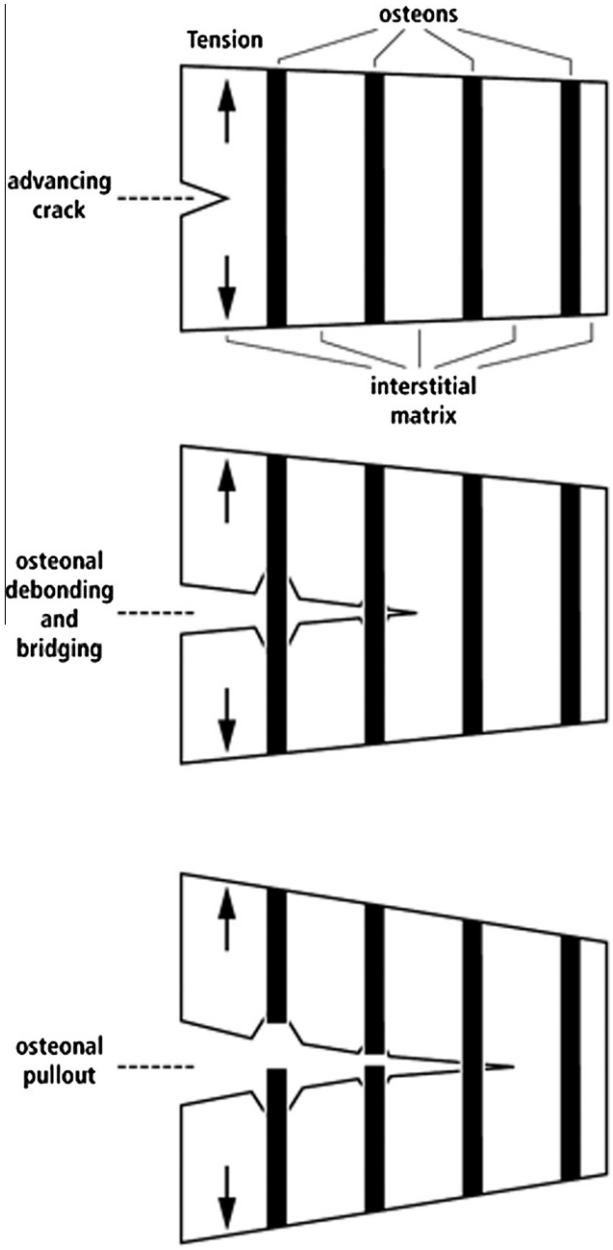

Fig.2. Diagrammatic representation of osteon pull-out in association with an advancing microcrack produced during tension loading. The osteons debond and then bridge the microcrack before they break; this enhances toughness by absorbing energy. Studies by Ritchie and co-workers (Launey et al., 2010a,b; Nalla et al., 2005b) suggest that this and other extrinsic mechanisms, which result in incomplete and largely extra-osteonal matrix breakage, do occur in natural conditions and can help to absorb energy. (Re-drawn and modified from Hiller et al. (2003).)

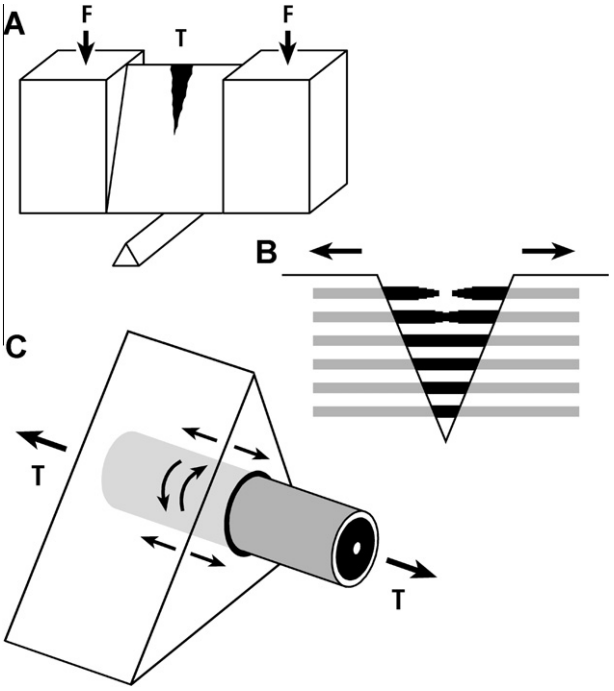

Fig.3. Osteon pull-out with interlamellar debonding ("telescoping") in tension loading. (A) Forces (F) applied to a machined specimen of cortical bone show a microcrack propagating downward across the specimen from the side loaded in tension (T). (B) Osteon pull-out and telescoping (in the two osteons at the top). (C) Higher magnified view of one of the hooped/parallel-fibered osteons shown in B. Here osteon pull-out is shown in addition to shear stresses (curved lines) in the cement line region (at the osteon periphery). This is believed to be common during bending in natural conditions. (Re-drawn and modified from Martin et al. (1998).)

lower strains)[2] (Hiller et al., 2003; Skedros, 2012; van Oers et al., 2008). Potentially adaptable relationships might exist between osteon size and morphotype because physiological loading is not simple, but it produces shear stresses that are potentially more deleterious than tension and compression stresses. In turn, shear stresses can be increased in the vicinity of the cement line when differential motion of the osteons occurs as the yield point is approached (Bigley et al., 2006; Ebacher et al., 2007; Leng et al., 2009; Pope and Murphy, 1974; Zimmermann et al., 2011). It has been speculated that this may help explain why osteons, especially in tension-loaded regions, often have a peripheral ring (or "hoop") of highly oblique/transverse collagen (Martin et al., 1996; Skedros et al., 2011b). In other words, this modification might help to resist deleterious consequences of these localized shear stresses, including excessive microdamage formation and propagation (Bigley et al., 2006; Mohsin et al., 2006; O'Brien et al., 2005; Skedros et al., 2005, 2009).

Osteonal debonding, bridging, and pullout have been identified as some of the extrinsic mechanisms that toughen cortical bone by controlling crack propagation and lowering the effective (local) stress intensity actually experienced at the crack tip (Bigley et al., 2006; Currey, 2002; Hiller et al., 2003; Launey et al., 2010a; Zimmermann et al., 2009) (Figs. 2 and 3). In this perspective, van Oers et al. (2008) offer a mechanically based explanation for why a functional relationship might exist between an osteon's morphotype and diameter:

> Osteon diameter affects the ratio between shear stress in the cement line and tensile stress on the osteon. Given a tensile force F on an osteon with diameter d and pullout length L, the tensile stress σ on the osteon and the shear stress τ in the cement line are given by: $\sigma = F/(\pi/4 \cdot d \cdot d)$ [or $\sigma = F/(\pi/(4d^2))$] and $\tau = F/(\pi \cdot d \cdot L)$. The ratio between σ and τ thus is $\tau/\sigma = d/4L$. [Pull-out occurs when $\sigma > \tau$.] Theoretically, pullout is thus more likely when osteons are larger in diameter, because this increases the shear stress in the cement line boundary relative to the tensile stress on the osteon (page 481).

[2] Strains only provide information about stresses if Young's modulus is known (Currey, 2002). Damage may be dependent on reaching a specific strain value, where here we imply that tension-loaded areas are more likely to fracture than compression-loaded areas especially if histomorphological adaptation for these habitual strain-mode differences does not occur. For the purposes of this discussion, tension and compression have been generalized in terms of strain; however, it must be recognized that these generalizations may not always be the case.

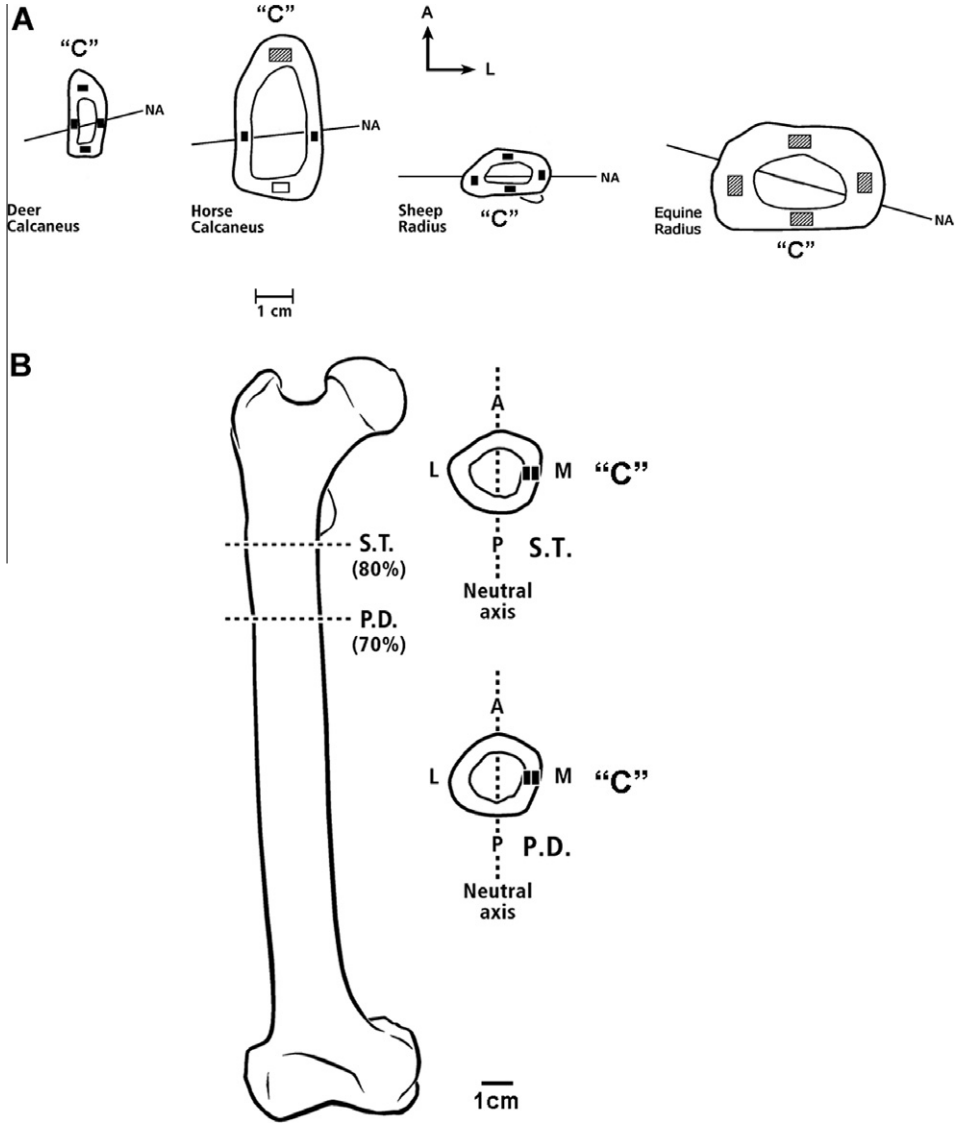

Fig.4. (A) Representative drawings of transverse cross-sections of the non-primate bones (adapted from (Skedros et al., 2009)). Small rectangles (shown in three sizes) within the cortices of these sections are locations where the analyses were conducted. Here "anterior" and "posterior", respectively, are used as surrogates for the actual, but various, terms used for the opposing sagittal-plane cortices in the calcanei (dorsal and plantar), radii (cranial and caudal), and equine MC3 (dorsal and palmar). Cr = cranial, anterior, or dorsal; L = lateral. NA = the estimated neutral axis. (B) Drawing of a right chimpanzee femur showing the two section locations, drawings of the representative transverse sections, and the four cortical locations that were examined in the primate femora (adapted from (Skedros et al., 2011a)). The small rectangles shown in the lateral cortices serve as examples of where the microscopic images were obtained in each of the four cortical locations. The dashed line drawn in the anterior-posterior direction shows the general location of the estimated neutral axis (NA) in the two sections. With respect to the NA, the medial cortex is in habitual compression (C) and the lateral cortex is habitual tension. A = anterior, L = lateral, P = posterior, M = Medial, ST = sub-trochanteric (80% diaphysis), PD = proximal diaphysis (70% diaphysis).

Consequently, in the "tension region" of a bone loaded in habitual bending there is an important tradeoff between potentially deleterious shear stresses at the cement line and the beneficial effects of increased osteon size. We hypothesized that this tradeoff would be recognized as increased "hoopedness" that would occur as an adaptation that resists deleterious shear stresses in cases where increased osteon diameter is mechanically advantageous—larger osteons in "tension" regions would be expected to have fully developed "hoops". The importance of this hypothesis is that, if supported, it suggests a coordination of different collagenous-matrix assembly activities between peripheral and subsequent deeper osteoblasts during osteon formation that are ultimately mechanically important. While this hypothesis has been considered by some investigators (Kerschnitzki et al., 2011; Marotti, 1996; Parfitt, 1983; Pazzaglia et al., 2011), it has not been tested in large samples of osteons from habitual bending environments and various species. We tested this hypothesis of size/hoop synergism by determining if there are significant correlations between osteon diameters and "hooped" morphotypes in "tension regions" *vs.* "compression regions" *vs.* "neutral axis regions" in a variety of limb bones.

2. Methods

The specimens and tissue preparation methods used in this study have been described in detail in previous studies (Skedros et al., 2009, 2011b). Briefly, circular polarized light (CPL) microscopic images were obtained at 50× from thin (100 μm) transverse sections from the following samples of adult primate and non-primate bones: (1) deer and equine calcanei, and sheep and equine radii ($n = 7$ of each bone type) (Skedros et al., 2009); (2) adult

chimpanzee femora ($n = 8$; mean age 25 years; age range: 18–31 years; 3 males; 4 females; one unknown sex) (Skedros et al., 2011b), and (3) modern adult human femora ($n = 12$; mean age: 53; age range: 22–71 years; 3 males; 9 females) (Skedros et al., 1999, 2012). All individuals were healthy prior to death and had no evidence of musculoskeletal disease, and they had not taken medications that could alter bone metabolism or remodeling activity.

CPL images in all of the bones were obtained in regions that corresponded to their typical mutually exclusive "tension", "compression", and "neutral axis" areas, as defined in previous studies (Skedros, 2012) (Fig. 4). In the non-primate bones, these locations were from the mid-shaft. In the human and chimpanzee femora these locations were from the proximal shaft where the bending moment is considered greatest (Skedros and Baucom, 2007).

The protocol was designed to select five complete osteons from each CPL image using a randomly oriented grid. However, there were instances where five osteons could not be selected using the grid because these images had relatively low osteon population density. This occurred in each species, and the frequency ranged from <0.1% in the equine calcanei (one osteon less than the maximum 385 osteons) to 8% in the human femora (81 less than the maximum 960 osteons). The mean area of each quantified osteon was directly measured from the digitized CPL image (ImageJ v. 1.43, National Institutes of Health, USA (Rasband, 1997–2009)). To facilitate consistency with published studies, osteon diameter is expressed as the mean of the maximum and minimum osteon diameters. This was sufficient for the purposes of this study because >95% of the osteons are quasi-circular. The "morphotype score" (MTS) of each complete osteon from non-human and chimpanzee bones had already been measured in the prior studies (where only the mean MTS of the entire image was previously reported). The MTSs for the human femur osteons were obtained for this study following the method described in the legend of Fig. 1.

The population densities of complete secondary osteons and the percent area of secondary osteonal bone had also been obtained for all images from each bone. Osteon population density was quantified as the number of complete secondary osteons in each image and divided by the area of each image (On.N/T.Ar; T.Ar = total image area including vascular spaces and osteocyte lacunae). The percent area of secondary bone ((On.B/T.Ar)·100); which includes complete and fragmentary osteons) was also quantified in each image. With the exception of the human femora, these data were obtained in our prior studies. Human femur data were collected according to our methods from previous studies, and inter- and intra-observer reliability was consistent with our previous studies (Skedros et al., 2009, 2011b).

2.1. Statistical analysis

A three-way analysis of covariance (ANCOVA) with Fisher's PLSD post hoc tests was used to evaluate the data in terms of: (1) morphotype score (MTS), (2) loading mode (i.e., habitual "tension", "compression", and "neutral axis/shear" regions), and (3) species (Table 1). The MTS score, which is actually an ordered categorical variable, was treated as a continuous variable in the ANCOVA, which results in a p-value that is interpreted as a linear trend test (Woodward, 2004). The 'species' distinction allowed for distinguishing between all bones, including equine radii and equine calcanei. Analyses then focused on osteon size (On.Dm) for all osteons (MTSs 0, 1, 2, 3, 4, and 5) and hooped osteons (MTSs 1, 2, 3, and 4) in terms of the three regions within each species. The osteon size cut-offs were defined as: (1) lower one-half and upper one-half of the range of osteon diameters within each bone type (size cut-off defined by mean value), and (2) <160, 161–209, and >210 μm. This latter grouping is based on data showing a bimodal distribution in the propensity for beneficial osteonal debonding and pullout in human and canine bone as suggested by the data of Moyle and co-workers (Moyle and Bowden, 1984; Moyle et al., 1978). In these studies, the energy absorption was higher when osteons are <160 and >210 μm diameter. In one case (deer calcaneus) where the number of osteons in each group was possibly insufficient for statistical analysis (15–47 osteons per group), the upper range was adjusted to >200 μm. Pearson correlations were used to assess potential relationships between osteon population density, diameter and MTS. Results of descriptive statistics of the osteon data are reported as means and standard deviations, which are based on values obtained from each image. The numbers of images and osteons quantified in each bone are indicated in data tables, as reported below. One-way ANOVA comparisons were used to determine if there are significant differences in osteon density and diameter between "tension regions" and "compression regions".

Table 1
ANCOVA table.

Factors	Degrees of Freedom	F Value	P value
Morphotype Score (MTS)	1	14.1	0.0002
Loading Mode	2	0.64	0.5
Species	5	3.35	0.005
MTS • Loading Mode	2	1.03	0.4
MTS • Species	5	1.66	0.14
MTS • Species • Loading **Mode**	10	1.13	0.3

Grayed cells represent statistical significance ($p < 0.05$).

3. Results

Results of the three-way ANCOVA showed significant effects of MTS and species (Table 1). There were statistically significant differences between most species comparisons ($p < 0.05$). Post-hoc analysis showed that osteon diameter tended to be greater in the hooped morphotypes 3 and 4 when compared to the hooped morphotypes 1 and 2. However, when considering all of the hooped osteons (MTSs 1–4) the results of paired comparisons based on small *vs.* large osteons showed that the hypothesized difference is suggested in only four of the six bone types (Fig. 5). Additionally, there was no case in either group where the expected difference was found in terms of the bimodal osteon-size relationship shown by Moyle and colleagues (Fig. 6). In other words, intermediate-size osteons did not have hooped MTSs that consistently differed from the small and large osteon groups (Fig. 6A).

The main hypothesis is also rejected by the results of the correlation analyses (Table 2) showing either weak or no relationships between osteon size and MTS. This is the case even when the analysis focused on the hooped osteons in the "tension" cortices of the

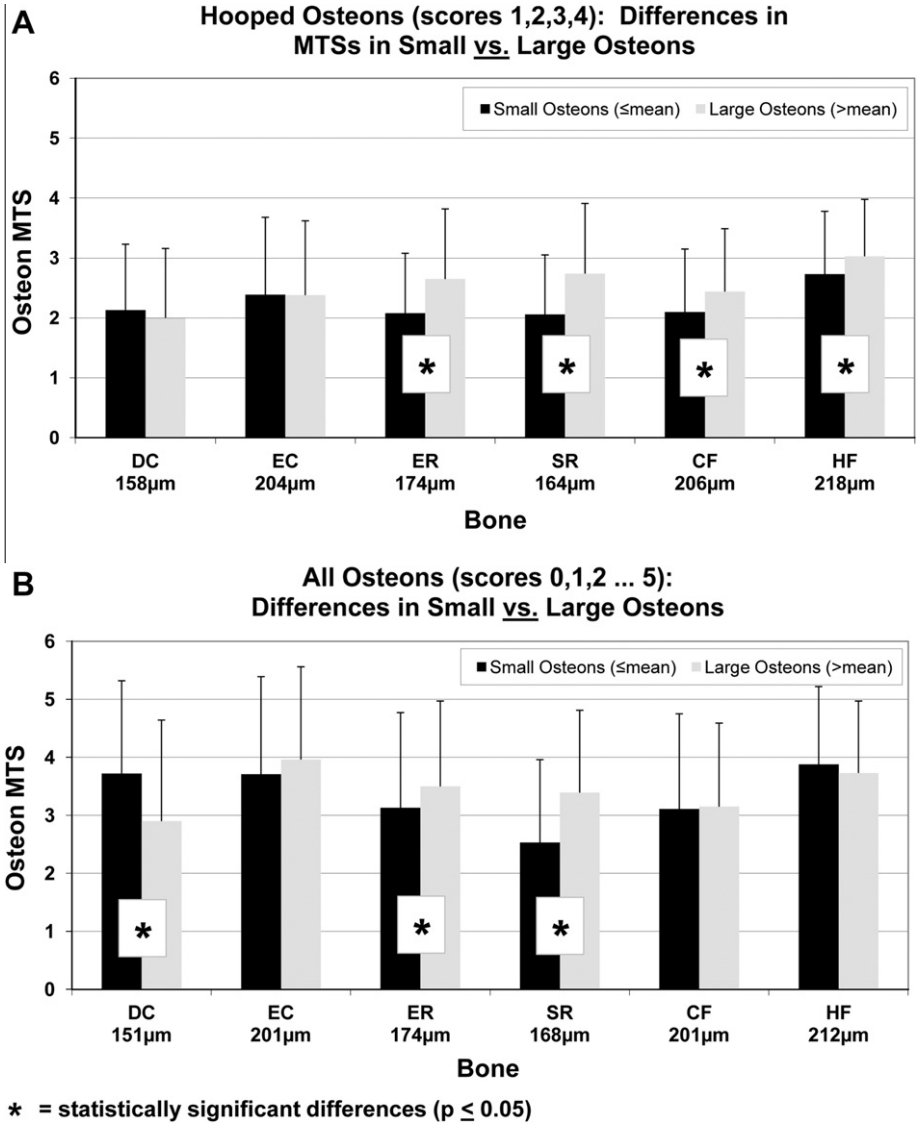

Fig.5. Results of paired comparisons based on the small *vs.* large osteon cut-off criterion. Results are shown for hooped osteons (A) and all osteons (B).

bones where the effect was expected to be most obvious (Table 2A). Examination of the variations in osteon size in each bone type revealed that they were sufficient to detect an effect of "hoopedness" had it been present in these analyses (Table 3A). Contrary to our expectations, the osteons are not consistently larger in the "tension regions" of all the bones (Table 3B).

Tables 3 and 4 also list data from each bone in terms of: (1) population density of complete osteons (On.N/T.Ar), (2) percent of each "hooped" morphotype, and (3) percent "hooped" morphotypes 1–2, and 1–3. Notably osteon morphotype 4 are relatively infrequent. Table 5 lists: (1) results of correlation analyses between On.N/T.Ar and osteon size (expressed as mean diameter, On.Dm), and (2) the area of secondary bone (On.B/T.Ar) data. Notably, not all of the On.N/T.Ar *vs.* On.Dm correlations are significant.

4. Discussion

The capacity of bones to undergo osteonal remodeling that results in regional differences in microstructural organization, which in turn produces corresponding differences in toughness of cortical bone, is an expected and common occurrence because the shafts of many limb bones are stereotypically loaded in bending during controlled ambulation (Skedros, 2012). In other words, these bones are loaded in such a way that one cortex is almost always loaded in compression while another cortex is almost always loaded in tension. The biomechanical importance of these regional microstructural adaptations can be understood by first considering the beneficial consequences of habitual bending. Bending produces a predictable strain distribution that is linked to predictable nutrient delivery and the production of other beneficial signals. These are essential for regional cell and tissue adaptation and homeostasis (e.g., strain gradients and fluid flux) (Bertram and Biewener, 1988; Robling, 2012; Skedros, 2012; Skedros et al., 1996). However, predictable bending also produces regional variations in strain history that are potentially deleterious because of the markedly non-equivalent mechanical properties and propensity for microfailure of cortical bone in the regions that receive prevalent/predominant compression, tension, and shear. For example, cortical bone is substantially stronger, tougher, and more fatigue resistant in compression than in tension or shear, and there is a propensity for the formation of longer microcracks in tension and smaller microcracks in compression (Boyce et al., 1998; Diab and Vashishth, 2007; Reilly and Currey, 1999; Reilly et al., 1997;

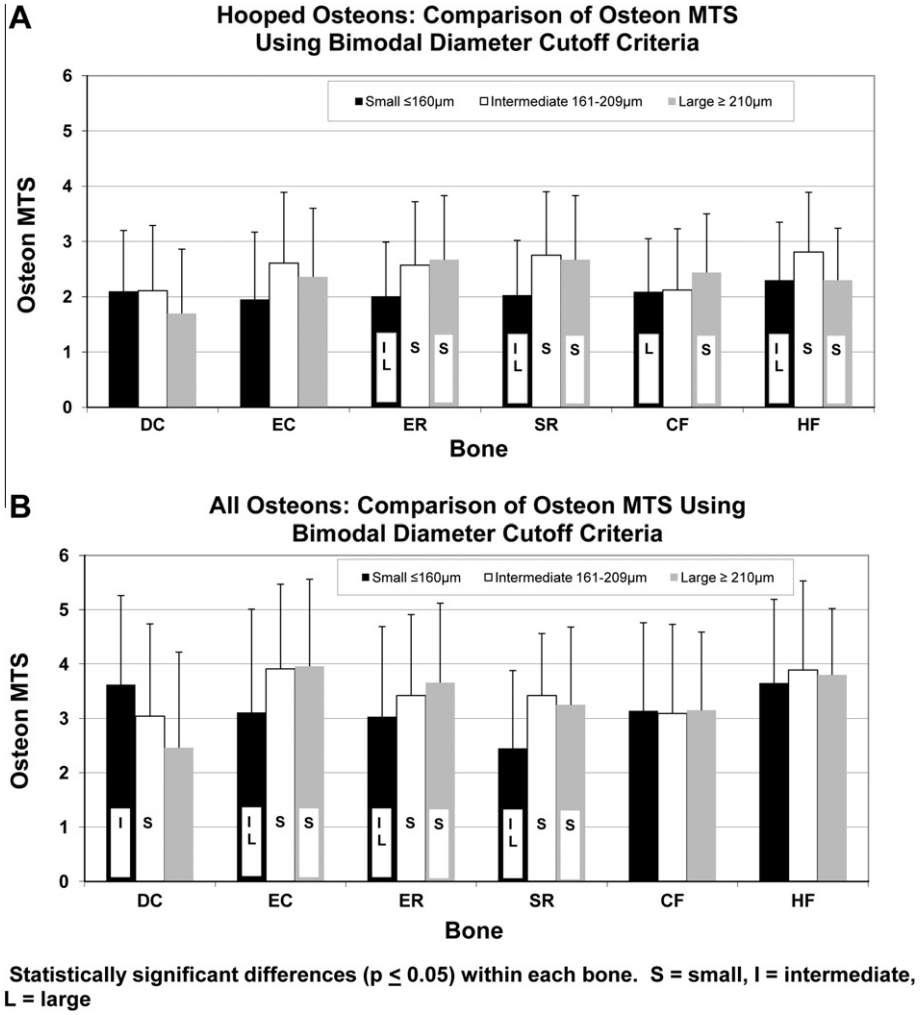

Fig.6. Results of comparisons using the three osteon-diameter groups. These are based on the bimodal distribution of osteon diameters that were found to enhance toughness in the studies of Moyle and colleagues (Moyle and Bowden, 1984; Moyle et al., 1978). See Section 2 for further description. Results are shown for hooped osteons (A) and all osteons (B).

Table 2
Results of correlation analyses in hooped osteons (A) and all osteons (B).

A

Bone	All Regions	"Compression" Cortex	"Tension" Cortex	"Neutral Axis"
Deer Calcaneus	-0.120	-0.535	0.132	-0.131
Equine Calcaneus	0.045	0.053	0.209	0.357
Equine Radius	0.274*	-0.212	0.242*	0.251*
Sheep Radius	0.303*	0.213	-0.052	0.442*
Chimp Femur	0.129	0.295*	0.175	0.067
Human Femur	0.224*	0.351*	0.159	0.179*

* p<0.05

B

Bone	All Regions	"Compression" Cortex	"Tension" Cortex	"Neutral Axis"
Deer Calcaneus	-0.225*	-0.223	0.014	-0.111
Equine Calcaneus	0.109	0.108	0.164	0.314*
Equine Radius	0.134	-0.029	0.232*	0.147*
Sheep Radius	0.296	0.217	-0.021	0.403*
Chimp Femur	0.003	0.117	0.046	-0.006
Human Femur	0.021	-0.011	-0.109	0.088

* p<0.05

Table 3
Osteon numbers, osteon population densities, and osteon diameters in hooped osteons (A) and all osteons (B). The Moyle classification is based on results of studies of human and canine bone (Moyle and Bowden, 1984; Moyle et al., 1978).

	Deer Calcaneus	Equine Calcaneus	Equine Radius	Sheep Radius	Chimp Femur	Human Femur
Number of Specimens	7	7	7	7	8	12
Number of Images	56	77	112	56	64	192
A. Hooped Osteons						
Size cutoff (mean of each bone)	158μm	204μm	174μm	164μm	206μm	218μm
Standard deviation	(42.2)	(48.2)	(40.2)	(41.8)	(65.8)	(52.3)
Range	80 - 339	115 - 336	97 - 283	79 - 271	68 - 453	99 - 358
No. Small (≤ mean)	77	78	169	116	117	257
No. Large (> mean)	70	70	177	95	101	236
Moyle Classification						
Small (≤160 μm)	84	26	134	109	58	53
Intermediate (161-209)	49 (43)*	60	154	72	61	134
Large (≥210 μm)	14 (20)*	61	58	29	99	306
B. All Osteons						
Size cutoff (mean of each bone)	151μm	210μm	174μm	168μm	201μm	212μm
Standard deviation	(40.9)	(48.0)	(40.9)	(42.5)	(63.0)	(51.9)
Range	76 - 339	109 - 372	93 - 283	75 - 304	65 - 453	99 - 390
No. Small (≤ mean)	156	201	271	144	175	474
No. Large (> mean)	113	183	278	128	145	405
Are osteons smaller in "compresson" vs. "tension" regions?‡	Y‡	Y‡	N‡ (C>T)	Y‡	Y‡	N‡ (C>T)
Is osteon population density greater in "compression" vs. "tension" regions?	Y‡	Y‡	Y‡	Y‡	N (C=T)	N (C=T)
Moyle Classification						
Small (≤160 μm)	176	50	211	130	92	106
Intermediate (161-209)	76 (67)*	151	236	103	97	261
Large (≥210 μm)	18 (27)*	183	102	39	131	512

C = Compression; T = Tension; Y = Yes; N = No.
‡These comparisons are statistically significant ($p < 0.05$).
*In these cases the number in parentheses was used, which was based on large osteons defined as >200 μm.

Skedros et al., 2006). It has been argued that these disparities explain why strain-mode-related variations in regional histomorphology are produced in bones loaded in habitual bending (Reilly and Currey, 1999; Skedros et al., 2007b, 2011b), especially in view of data showing that longer microcracks are relatively more deleterious than shorter microcracks (Mohsin et al., 2006; O'Brien et al., 2005) (Fig. 7). Consequently, we predicted that a coupling of osteon size and morphotype would occur as an adaptation that ultimately curbs and/or accommodates the propensity to incur regional variations in the amounts and types of microdamage that can be an untoward consequence of regionally non-uniform strains. As discussed below, while the results of this study do not support this hypothesis, the data reveal other potentially important relationships between specific osteon morphological characteristics and strain history. van Oers et al. (2008) and other investigators have argued that small resorption spaces and the small osteons that are subsequently produced are adaptations that are most ideal in highly strained areas, which are usually the "compression regions" in directionally consistent (habitual) bending environments (Britz et al., 2009; Lieberman et al., 2003; Martin et al., 1996; Skedros et al., 2001, 2007b, 2009; van Oers et al., 2008). However, van Oers et al. (2008) did not distinguish between osteon-based microfailure mechanisms in cases where there are clear regional differences in habitual strain mode, which exposes a problem in their arguments. They discuss how osteon diameter can affect debonding/pullout in terms of tension-based microfailure events even though their data are derived from a computational model of osteon formation in compression environments. In compression, the relevance of pullout is relatively less important. In fact, previous experimental studies have shown that: (1) shear deformation (cross hatched microcracks) is the major mechanism of the post-yield deformation of human cortical bone in compression, and (2) the local shear deformation in oblique orientations may actually dominate the microdamage accumulation and

Table 4
Percentages of hooped osteon morphotypes in "tension regions".

	1	2	3	4	1-2	1-3
A. Hooped Osteons Only						
Deer Calcaneus (Plantar)	72%	16%	11%	1%	88%	99%
Equine Calcaneus (Plantar)	70%	18%	7%	5%	87%	95%
Equine Radius (Cranial)	29%	54%	4%	12%	84%	88%
Sheep Radius (Cranial)	27%	28%	26%	19%	55%	81%
Chimpanzee Femur (Lateral)	32%	26%	28%	15%	58%	85%
Human Femur (Lateral)	24%	22%	39%	15%	46%	85%
B. All Osteons						
Deer Calcaneus (Plantar)	51%	11%	8%	>1%	62%	70%
Equine Calcaneus (Plantar)	60%	15%	6%	5%	75%	81%
Equine Radius (Cranial)	25%	46%	3%	11%	72%	75%
Sheep Radius (Cranial)	20%	20%	19%	14%	40%	59%
Chimpanzee Femur (Lateral)	23%	18%	20%	10%	42%	62%
Human Femur (Lateral)	13%	12%	22%	8%	25%	47%

Grayed cells show percentage of hooped morphotype scores 1–3 out of all hooped osteons. Note, these are substantially larger than the percentage of the hooped morphotype score 4.

Table 5
Correlations of osteon population density (On.N/T.Ar) *vs.* osteon size (expressed here as osteon diameter, On.Dm) for all osteon morphotypes. Also shown are descriptive data for On.N/T.Ar, On.Dm, and the fractional area of secondary bone expressed as a percentage ((On.B/T.Ar) × 100). The majority of these data used for these correlation analyses are from Skedros et al. (2009).

	Correlation of On.N/T.Ar *vs.* On.Dm		On.N/T.Ar (no./mm^2)	ON.Dm (μm)	(On.B/T.Ar)«100
	r	*p*			
Deer calcaneus (*n* = 7)	−0.34	0.03			
No. images = 56					
No. osteons = 269					
Mean			25.1	151	39%
Std dev			19.9	40.9	28%
Range			0.–56.9	76–339	1–85%
Equine calcaneus (*n* = 7)	−0.56	<0.001			
No. images = 77					
No. osteons = 384					
Mean			17.6	210	73%
Std dev			4.9	48.0	9%
Range			9.8–31.1	109–372	39–92%
Equine radius (*n* = 7)	−0.15	0.2			
No. images = 112					
No. osteons = 549					
Mean			12.6	174	35%
Std dev			6.1	40.9	20%
Range			2.0–24.2	93–283	5–75%
Sheep radius (*n* = 7)	−0.20	0.2			
No. images = 56					
No. osteons = 272					
Mean			19.6	168	44%
Std dev			8.6	42.5	21%
Range			0.7–36.0	75–304	2–91%
Chimp femur (*n* = 8)	−0.43	<0.001			
No. images = 64					
No. osteons = 320					
Mean			15.8	201	71%
Std dev			3.6	63.0	23%
Range			7.5–26.4	65–453	11–100%
Human femur (*n* = 12)	−0.60	<0.001			
No. images = 192					
No. osteons = 879					
Mean			15.6	212	NA
Std dev			4.5	51.9	
Range			5.6–28.9	99–390	

NA = data not available; Std dev = standard deviation; No. = number.

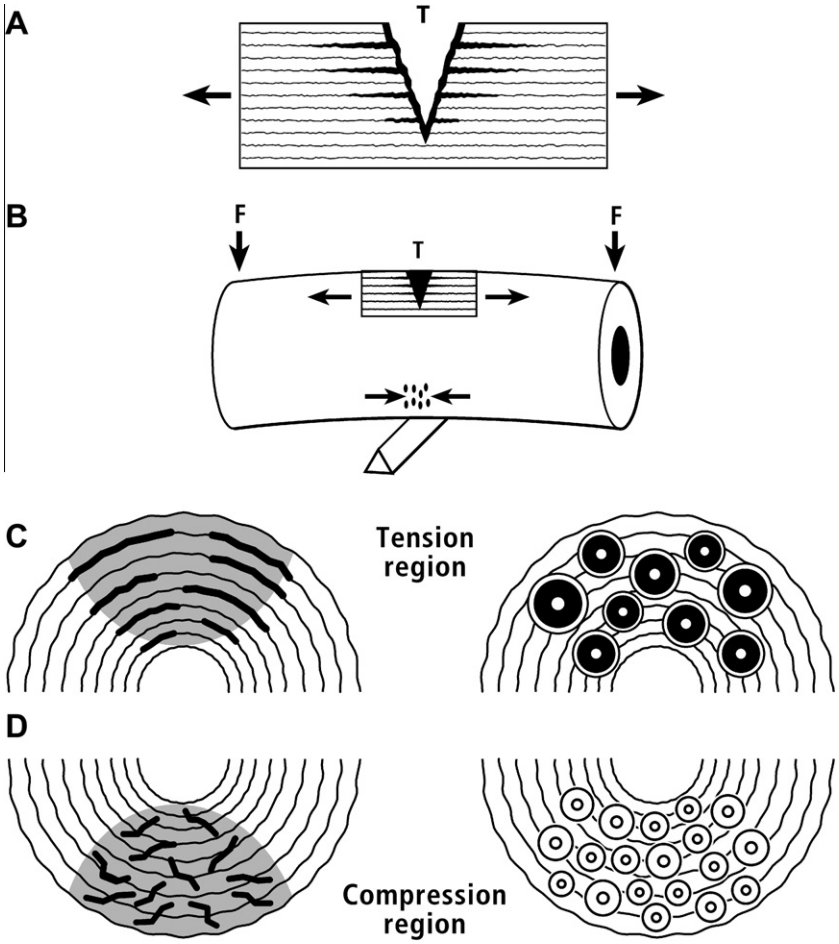

Fig.7. A diagrammatic representation of a region (A) within the tension (T) side of a bone shaft (B) cyclically loaded in bending in a directionally consistent manner. The V-shaped crack on the top in A and B (exaggerated in size) corresponds to the region with the longer microcracks in the grayed damage zone in C. The osteons that subsequently form are larger and are adapted for the ambient tension (i.e., consistent with our hypothesis they are large, have predominantly longitudinal collagen and strong/complete hoops). On the opposite (compression) side of the bone, the smaller microcracks in compression are formed (D), and these are repaired by smaller osteons that are also adapted for the ambient compression (i.e., they are distributed/alternating morphotypes).

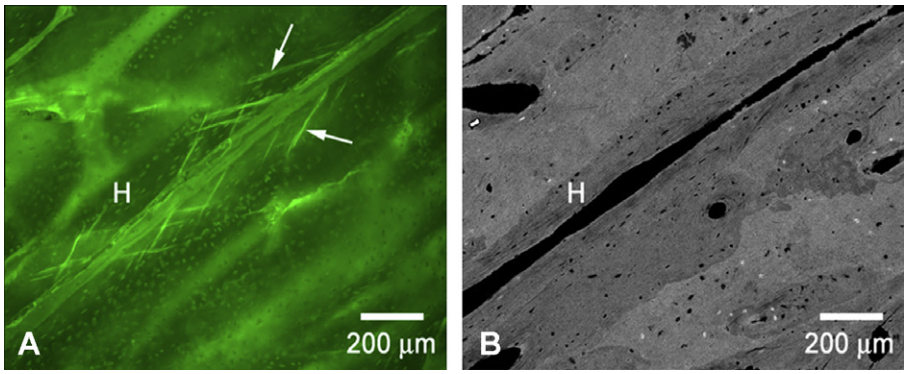

Fig.8. Cross-hatching (shear-type) microdamage entities (also known as "slip" failure lines) that formed during compression loading. Shown is a lateral view of an individual secondary osteon (Haversian system, H) visualized under epi-fluorescense mode (A) and the corresponding backscattered electron image (B). Compressive stress was applied along top/right to bottom/left axis of the images. The arrows indicate two of the shear-type microcracks. (Re-produced by Ebacher et al. (2007) with permission of Elsevier).

post-yield behavior of bone in compression (Ebacher et al., 2007; Leng et al., 2009) (Fig. 8). This starkly contrasts with the debonding/pullout mechanisms that occur in tension microfailure (Figs. 3 and 9). Consequently, it is essential that the distribution of strain mode is considered when interpreting the potential adaptive relevance of regional variations in osteon prevalence, size, and matrix lamellar/collagen organization. This is important when considering the differences in the mechanically adaptive toughening mechanisms conferred by hooped (i.e., "tension adapted") morphotypes (scores 1, 2, 3, 4) *vs.* the bright/alternating ("compression adapted") morphotype (score 5) (Bigley et al., 2006; Hiller et al., 2003; Skedros et al., 2011b). It has been speculated that increased

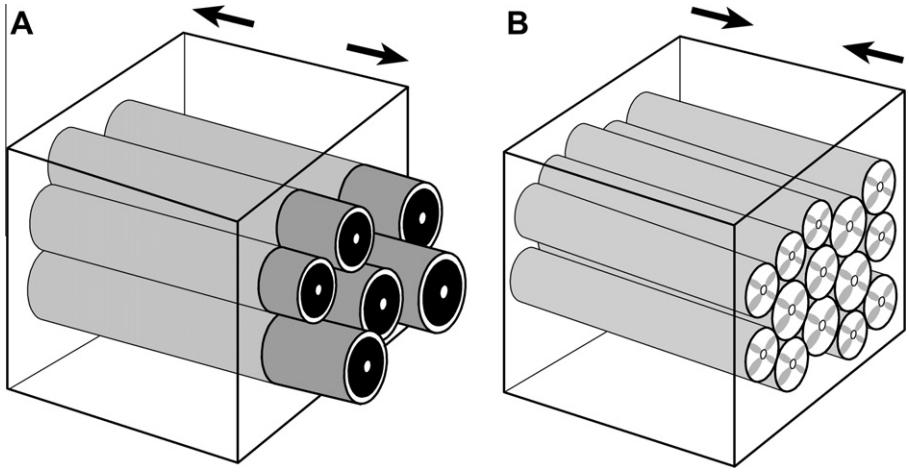

Fig.9. (A) A diagram of a magnified block of bone showing tension-adapted osteons (i.e., hooped/parallel-fibered) exhibiting pull-out in tension failure. (B) A diagram of a magnified block of bone showing compression-adapted osteons with oblique "slip" failure lines that represent the shear-type microdamage seen in compression failure. These "slip" failure lines are seen in lateral view in an actual osteon in Fig. 7.

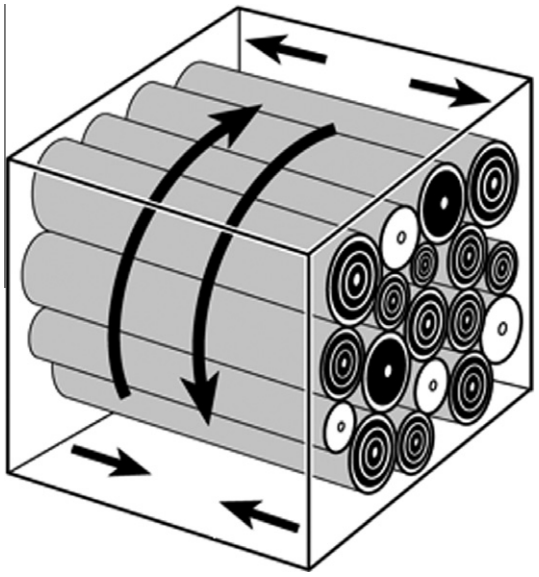

Fig.10. Diagram of a magnified block of bone showing various osteon morphotypes, including "hybrids" (see columns 2 and 3 in Fig. 1) that are believed to be well suited for accommodating heterogeneous strains produced by variable/complex loading environments. The arrows pointing toward each other represent compression, the arrows pointing away from each other represent tension, and the curved arrows represent twisting/torsion.

morphotype heterogeneity and/or morphotypes that are "hybrids" of hooped and bright/alternating (Skedros et al., 2011b) might be mechanically advantageous in complex load environments where it has been argued that the differential movement of the osteon and its matrix in the direction of the load increases shear stresses in the cement line region (Bigley et al., 2006; Martin et al., 1998) (Figs. 3 and 10).

Although several studies suggest that there is an inverse relationship between osteon size (diameter) and strain magnitude, there are notable exceptions. For example, the more highly strained caudal "compression" cortex of our equine radii have osteons that are significantly larger than those in the cranial "tension" cortex where strains are also relatively lower (B). In a different sample of horse radii, Mason et al. (1995) also showed that the osteons in the caudal "compression" cortex are not significantly smaller than those in the opposing cranial "tension" cortex. A study of equine MC3s also did not find a significant difference in osteon size between the medial and lateral regions (Skedros et al., 2009), which are also high and low strain environments, respectively (Skedros et al., 1996). These regions can also be distinguished by relatively habitual compression medially *vs.* tension laterally, and regional differences in the prevalence of osteon morphotypes do correspond to this strain history (Martin et al., 1996; Skedros et al., 2006, 2009).

In some cases our data seem to suggest a fairly strong relationship between osteon density and loading mode, and possibly even between osteon population density (On.N/T.Ar) and size (Tables 3 and 5). While consistent with some prior studies, these are not universal findings. For example, in a study of human femora from elderly cadavers, Yeni et al. (1997) found that osteon size is negatively related to fracture toughness while osteon population density has a positive relationship with this property. While this suggests that an effect of osteon size is possibly a function of osteon population density, this relationship was not found in their sample of adult human tibiae. Data in our Tables 3 and 5 show that osteon population density is not consistently associated with osteon size or habitual strain mode. In fact, the correlations between osteon population density and mean diameter (On.Dm) from the present study showed weak-to-moderate correlations in some bones and no correlations in others (Table 5). In contrast with our analysis, Yeni and co-workers did not consider the possibility that osteon morphotypes played a role in this context or the possibility that there could be regional strain-mode-related microstructural adaptations. If we assume that different osteon morphotypes had no effect on Yeni and co-workers' conclusions in their femur sample, then it is likely that smaller osteons improve fatigue properties by being strongly linked to increased osteon population density in the cortical regions that they studied. In other words, their data suggest that a large number of smaller osteons will be more efficient than a small number of larger osteons in reducing the effect of damage accumulation (Donahue and Galley, 2006; Mohsin et al., 2006; Norman and Wang, 1997; O'Brien et al., 2005; Wasserman et al., 2008; Zimmermann et al., 2009). This is probably because cement lines effectively serve as a barrier to crack propagation, and the smaller microcracks that ultimately form are mechanically less deleterious than long microcracks (Mohsin et al., 2006; O'Brien et al., 2005).

While the present (Table 3) and past studies show that osteon size is not consistently related to ambient strain magnitude, there are data suggesting that regional variations in predominant CFO

(often produced by osteon morphotypes) are more strongly correlated with strain mode (Mason et al., 1995; Riggs et al., 1993a; Skedros et al., 2009, 2011b). In fact, the association of regional variations in predominant CFO and/or osteon morphotypes with the distribution of net tension and compression strains of habitual bending has been shown to be much more consistent than either osteon size or population density (Skedros, 2012; Skedros et al., 2009). When considering evidence that predominant CFO is causally related to strain mode and not strain magnitude (Takano et al., 1999), and the fact that our results do not support our hypothesis that osteon diameter is coupled with osteon morphotype, it is clear that further research is needed to address some of the additional hypotheses raised by our study. For example, it is not known if the higher prevalence of osteon morphotypes 1, 2, and 3 than morphotype 4 (Table 4) is mechanically adaptive in some load environments. In other words, it is not known if the degree of "hoopedness" plays a mechanically important role. Additional research should determine if osteon size and MTS are mediated by different stimuli.

Limitations of our study include the designation of habitual strain-mode regions in some bones where this distinction is less clear than in others because of their differences in loading variability/complexity. This is the case in the proximal shaft locations of the primate bones when compared to the mid-shaft locations of non-primate bones used in this study (Skedros, 2012). Nevertheless, as reported in previous studies, the predominant CFO patterns in all bones examined in the present study show significant differences that are consistent with habitual bending (i.e., more oblique-to-transverse CFO in "compression regions" and more longitudinal CFO in "tension" regions) (Boyde and Riggs, 1990; Riggs et al., 1993a; Skedros et al., 1999, 2009, 2011b). Additionally, the hypothesis that osteon size and hoopedness are coupled was still rejected even in the more simply loaded calcanei and radii. Another limitation of this study is that it cannot determine causal relationships between osteon morphological characteristics; it can only address associations.

In summary, the results of this study show that osteon size and morphotype are not coupled in the bones and regions that we examined. But some of the results of the present and prior studies suggest that these osteon characteristics have the potential for independent adaptations for locally prevalent/predominant strain mode or magnitude. However, among the various bone types studied, the associations of osteon size with strain magnitude and osteon population density are inconsistent. This contrasts with the more consistent association of osteon morphotypes with a regionally prevalent/predominant strain mode. Consequently, osteon MTSs and the predominant CFO variations that they produce are comparatively stronger correlates of spatially non-uniform strain-mode histories produced by habitual bending, which is a common load history in many limb bones. It is also clear that osteonal adaptations for microfailure mechanisms cannot be generic in non-uniform load environments because marked differences would be expected for the locally prevalent/predominant strain modes that are produced.

Acknowledgments

The authors thank Erick Anderson, Kyle Gubler, Jaxon Hoopes, Scott Sorenson, Adam Beckstrom, Anna Adondakis, and Chase Jardine for their assistance in completing this study. We are indebted to Pat Campbell and Harlan Amstutz for the use of their laboratory facilities at the Joint Replacement Institute of Orthopaedic Hospital in Los Angeles, California. This research is supported by USA Department of Veterans Affairs medical research funds, and the Doctor's Education Research Fund (DERF) of Orthopaedic Hospital, Los Angeles, California, USA.

References

Bertram, J.E., Biewener, A.A., 1988. Bone curvature: sacrificing strength for load predictability? J. Theor. Biol. 131, 75–92.
Bigley, R.F., Griffin, L.V., Christensen, L., Vandenbosch, R., 2006. Osteonal interfacial strength and histomorphometry of equine cortical bone. J. Biomech. 39, 1629–1640.
Boyce, T.M., Fyhrie, D.P., Glotkowski, M.C., Radin, E.L., Schaffler, M.B., 1998. Damage type and strain mode associations in human compact bone bending fatigue. J. Orthop. Res. 16, 322–329.
Boyde, A., Riggs, C.M., 1990. The quantitative study of the orientation of collagen in compact bone slices. Bone 11, 35–39.
Britz, H.M., Thomas, C.D., Clement, J.G., Cooper, D.M., 2009. The relation of femoral osteon geometry to age, sex, height and weight. Bone 45, 77–83.
Bromage, T.G., Goldman, H.M., McFarlin, S.C., Warshaw, J., Boyde, A., et al., 2003. Circularly polarized light standards for investigations of collagen fiber orientation in bone. Anat. Rec. 274B, 157–168.
Crescimanno, A., Stout, S.D., 2012. Differentiating fragmented human and nonhuman long bone using osteon circularity. J. Forensic Sci. 57, 287–294.
Currey, J.D., 2002. Bones: Structure and Mechanics. Princeton University Press, Princeton, NJ.
Diab, T., Vashishth, D., 2007. Morphology, localization and accumulation of *in vivo* microdamage in human cortical bone. Bone 40, 612–618.
Doblaré, M., García Aznar, J.M., Gómez, M.J., 2004. Modelling bone tissue fracture and healing: a review. Eng. Fract. Mech. 71, 1809–1840.
Donahue, S.W., Galley, S.A., 2006. Microdamage in bone: implications for fracture, repair, remodeling, and adaptation. Crit. Rev. Biomed. Eng. 34, 215–271.
Ebacher, V., Tang, C., McKay, H., Oxland, T.R., Guy, P., et al., 2007. Strain redistribution and cracking behavior of human bone during bending. Bone 40, 1265–1275.
Hiller, L.P., Stover, S.M., Gibson, V.A., Gibeling, J.C., Prater, C.S., et al., 2003. Osteon pullout in the equine third metacarpal bone: effects of *ex vivo* fatigue. J. Orthop. Res. 21, 481–488.
Hogan, H.A., 1992. Micromechanics modeling of Haversian cortical bone properties. J. Biomech. 25, 549–556.
Keenan, K., Knight, A., Tingey, S., Kiser, C., Thomas, S., et al., 2010. Drifting osteons occur in higher concentrations in habitual tension environments: a microstructural toughening mechanism? Am. J. Phys. Anthropol. Suppl. 50, 140.
Kerschnitzki, M., Wagermaier, W., Roschger, P., Seto, J., Shahar, R., et al., 2011. The organization of the osteocyte network mirrors the extracellular matrix orientation in bone. J. Struct. Biol. 173, 303–311.
Launey, M.E., Buehler, M.J., Ritchie, R.O., 2010a. On the mechanistic origins of toughness in bone. Annu. Rev. Mater. Res. 40, 25–53.
Launey, M.E., Chen, P.Y., McKittrick, J., Ritchie, R.O., 2010b. Mechanistic aspects of the fracture toughness of elk antler bone. Acta Biomater. 6, 1505–1514.
Leng, H., Dong, X.N., Wang, X., 2009. Progressive post-yield behavior of human cortical bone in compression for middle-aged and elderly groups. J. Biomech. 42, 491–497.
Lieberman, D.E., Pearson, O.M., Polk, J.D., Demes, B., Crompton, A.W., 2003. Optimization of bone growth and remodeling in response to loading in tapered mammalian limbs. J. Exp. Biol. 206, 3125–3138.
Marotti, G., 1996. The structure of bone tissues and the cellular control of their deposition. Ital. J. Anat. Embryol. 101, 25–79.
Martin, R.B., Gibson, V.A., Stover, S.M., Gibeling, J.C., Griffin, L.V., 1996. Osteonal structure in the equine third metacarpus. Bone 19, 165–171.
Martin, R.B., Burr, D.B., Sharkey, N.A., 1998. Skeletal Tissue Mechanics. Springer-Verlag, New York, NY.
Mason, M.W., Skedros, J.G., Bloebaum, R.D., 1995. Evidence of strain-mode-related cortical adaptation in the diaphysis of the horse radius. Bone 17, 229–237.
Mohsin, S., O'Brien, F.J., Lee, T.C., 2006. Osteonal crack barriers in ovine compact bone. J. Anat. 208, 81–89.
Moyle, D.D., Bowden, R.W., 1984. Fracture of human femoral bone. J. Biomech. 17, 203–213.
Moyle, D.D., Welborn 3rd, J.W., Cooke, F.W., 1978. Work to fracture of canine femoral bone. J. Biomech. 11, 435–440.
Najafi, A., Arshi, A., Saffar, K., Eslami, M., Fariborz, S., et al., 2009. A fiber-ceramic matrix composite material model for osteonal cortical bone fracture micromechanics: solutions of arbitrary microcracks interaction. J. Mech. Behav. Biomed. Mater. 2, 217–223.
Nalla, R.K., Stolken, J.S., Kinney, J.H., Ritchie, R.O., 2005a. Fracture in human cortical bone: local fracture criteria and toughening mechanisms. J. Biomech. 38, 1517–1525.
Nalla, R.K., Kruzic, J.J., Kinney, J.H., Ritchie, R.O., 2005b. Mechanistic aspects of fracture and R-curve behavior in human cortical bone. Biomaterials 26, 217–231.
Norman, T.L., Wang, Z., 1997. Microdamage of human cortical bone: incidence and morphology in long bones. Bone 20, 375–379.
O'Brien, F., Taylor, D., Lee, T.C., 2005. The effect of bone microstructure on the initiation and growth of microcracks. J. Orthop. Res. 23, 475–480.
Parfitt, A.M., 1983. The physiologic and clinical significance of bone histomorphometric data. In: Recker, R.R. (Ed.), Bone Histomorphometry: Techniques and Interpretation. CRC Press, Inc., Boca Raton, pp. 143–224 (Chapter 9).
Pazzaglia, U.E., Congiu, T., Zarattini, G., Marchese, M., Quacci, D., 2011. The fibrillar organisation of the osteon and cellular aspects of its development : a morphological study using the SEM fractured cortex technique. Anat. Sci. Int. 86, 128–134.

Pope, M.H., Murphy, M.C., 1974. Fracture energy of bone in a shear mode. Med. Biol. Eng. 12, 763–767.
Rasband, W., 1997–2009. ImageJ, 1.43 ed. U.S. National Institutes of Health, Bethesda, Maryland.
Reilly, G.C., Currey, J.D., 1999. The development of microcracking and failure in bone depends on the loading mode to which it is adapted. J. Exp. Biol. 202, 543–552.
Reilly, G.C., Currey, J.D., Goodship, A., 1997. Exercise of young thoroughbred horses increases impact strength of the third metacarpal bone. J. Orthop. Res. 15, 862–868.
Riggs, C.M., Lanyon, L.E., Boyde, A., 1993a. Functional associations between collagen fibre orientation and locomotor strain direction in cortical bone of the equine radius. Anat. Embryol. 187, 231–238.
Riggs, C.M., Vaughan, L.E., Boyde, A., Lanyon, L.E., 1993b. Mechanical implications of collagen fibre orientation in cortical bone of the equine radius. Anat. Embryol. 187, 239–248.
Robling, A.G., 2012. The interaction of biological factors with mechanical signals in bone adaptation: recent developments. Curr. Osteoporos Rep. 10, 126–131.
Robling, A.G., Stout, S.D., 1999. Morphology of the drifting osteon. Cells Tissues Organs 164, 192–204.
Skedros, J.G., 2012. Interpreting load history in limb–bone diaphyses: important considerations and their biomechanical foundations. In: Crowder, C., Stout, S. (Eds.), Bone Histology: An Anthropological Perspective. CRC Press, Boca Raton, Florida, pp. 153–220.
Skedros, J.G., Baucom, S.L., 2007. Mathematical analysis of trabecular 'trajectories' in apparent trajectorial structures: the unfortunate historical emphasis on the human proximal femur. J. Theor. Biol. 244, 15–45.
Skedros, J.G., Mason, M.W., Nelson, M.C., Bloebaum, R.D., 1996. Evidence of structural and material adaptation to specific strain features in cortical bone. Anat. Rec. 246, 47–63.
Skedros, J.G., Hughes, P.E., Nelson, K., Winet, H., 1999. Collagen fiber orientation in the proximal femur: challenging Wolff's tension/compression interpretation. J. Bone Miner. Res. 14, S441.
Skedros, J.G., Mason, M.W., Bloebaum, R.D., 2001. Modeling and remodeling in a developing artiodactyl calcaneus: a model for evaluating Frost's mechanostat hypothesis and its corollaries. Anat. Rec. 263, 167–185.
Skedros, J.G., Holmes, J.L., Vajda, E.G., Bloebaum, R.D., 2005. Cement lines of secondary osteons in human bone are not mineral-deficient: new data in a historical perspective. Anat. Rec. A Discov. Mol. Cell. Evol. Biol. 286, 781–803.
Skedros, J.G., Dayton, M.R., Sybrowsky, C.L., Bloebaum, R.D., Bachus, K., 2006. The influence of collagen fiber orientation and other histocompositional characteristics on the mechanical properties of equine cortical bone. J. Exp. Biol. 209, 3025–3042.
Skedros, J.G., Sorenson, S.M., Jenson, N.H., 2007a. Are distributions of secondary osteon variants useful for interpreting load history in mammalian bones? Cells Tissues Organs 185, 285–307.
Skedros, J.G., Sorenson, S.M., Hunt, K.J., Holyoak, J.D., 2007b. Ontogenetic structural and material variations in ovine calcanei: a model for interpreting bone adaptation. Anat. Rec. 290, 284–300.
Skedros, J.G., Mendenhall, S.D., Kiser, C.J., Winet, H., 2009. Interpreting cortical bone adaptation and load history by quantifying osteon morphotypes in circularly polarized light images. Bone 44, 392–403.
Skedros, J.G., Kiser, C.J., Mendenhall, S.D., 2011a. A weighted osteon morphotype score out-performs regional osteon percent prevalence calculations for interpreting cortical bone adaptation. Am. J. Phys. Anthropol. 144, 41–50.
Skedros, J.G., Kiser, C.J., Keenan, K.E., Thomas, S.C., 2011b. Analysis of osteon morphotype scoring schemes for interpreting load history: evaluation in the chimpanzee femur. J. Anat. 218, 480–499.
Skedros, J.G., Keenan, K.E., Halley, J.A., Knight, A.N., Bloebaum, R.D., 2012. Osteon morphotypes and predominant collagen fiber orientation are adaptations for habitual medial-lateral bending in the human proximal diaphysis: implications for understanding the etiology of atypical fractures. 58th Annual Meeting of the Orthopaedic Research Society, vol. 37, p. 1512.
Takano, Y., Turner, C.H., Owan, I., Martin, R.B., Lau, S.T., et al., 1999. Elastic anisotropy and collagen orientation of osteonal bone are dependent on the mechanical strain distribution. J. Orthop. Res. 17, 59–66.
Turner, C.H., Burr, D.B., 1993. Basic biomechanical measurements of bone: a tutorial. Bone 14, 595–608.
van Oers, R.F., Ruimerman, R., van Rietbergen, B., Hilbers, P.A., Huiskes, R., 2008. Relating osteon diameter to strain. Bone 43, 476–482.
Vashishth, D., 2004. Rising crack-growth-resistance behavior in cortical bone: implications for toughness measurements. J. Biomech. 37, 943–946.
Wasserman, N., Brydges, B., Searles, S., Akkus, O., 2008. *In vivo* linear microcracks of human femoral cortical bone remain parallel to osteons during aging. Bone 43, 856–861.
Woodward, M., 2012. Epidemiology: Study Design and Data Analysis, second ed. Chapman and Hall/CRC, New York.
Yeni, Y.N., Brown, C.U., Wang, Z., Norman, T.L., 1997. The influence of bone morphology on fracture toughness of the human femur and tibia. Bone 21, 453–459.
Zimmermann, E.A., Launey, M.E., Barth, H.D., Ritchie, R.O., 2009. Mixed-mode fracture of human cortical bone. Biomaterials 30, 5877–5884.
Zimmermann, E.A., Schaible, E., Bale, H., Barth, H.D., Tang, S.Y., et al., 2011. Age-related changes in the plasticity and toughness of human cortical bone at multiple length scales. Proc. Natl. Acad. Sci. USA 108, 14416–14421.
Zioupos, P., Currey, J.D., 1998. Changes in the stiffness, strength, and toughness of human cortical bone with age. Bone 22, 57–66.